Journal of Power Sources 220 (2012) 269–279

Contents lists available at SciVerse ScienceDirect

Journal of Power Sources

journal homepage: www.elsevier.com/locate/jpowsour

Electrochemical performance of microbial fuel cells based on disulfonated poly(arylene ether sulfone) membranes

Tae Hwan Choi [a], Young-Bin Won [b], Jin-Won Lee [b], Dong Won Shin [a], Young Moo Lee [a], Minkyong Kim [c], Ho Bum Park [a,*]

[a] WCU Department of Energy Engineering, Hanyang University, 17 Haengdang-dong, Seongdong-gu, Seoul 133-791, Republic of Korea
[b] Department of Biology, Hanyang University, Seoul 133-791, Republic of Korea
[c] Department of Chemistry, Hanyang University, Seoul 133-791, Republic of Korea

HIGHLIGHTS

- Microbial fuel cells based on newly synthesized hydrocarbon-based polyelectrolyte membranes.
- Disulfonated poly(ether sulfone) membranes can be used for MFC applications.
- Degree of sulfonation is a key factor to affect electrochemical performance in MFCs.

ARTICLE INFO

Article history:
Received 24 April 2012
Received in revised form
17 June 2012
Accepted 31 July 2012
Available online 8 August 2012

Keywords:
Fuel Cells
Microbial fuel cell
Polymer electrolyte membrane
Sulfonated polymer membrane

ABSTRACT

A microbial fuel cell (MFC) is a bio-electrochemical system that drives a current by mimicking bacterial interactions found in nature. Usually, MFCs use Nafion as a PEM to separate the electrodes while permitting protons transfer between the anode and cathode. However, Nafion is expensive and accounts for a large percentage of the costs in MFC configuration. Here, we show MFCs using hydrocarbon-based PEM, disulfonated poly (arylene ether sulfone) (BPSH), which is considered as one of alternative PEM, and relatively inexpensive as compared with Nafion. BPSH membranes exhibit a comparable performance to Nafion 212. Especially, BPSH 40 and 60 (mole %) have higher proton conductivity than Nafion 212. In a two-chamber system, MFC with BPSH 40 shows higher voltage than that with Nafion 212. MFCs with BPSH 20 and 30 show lower voltage decline than other PEMs. In a single-chamber system, a voltage of MFC with BPSH 40 shows about 30% higher (17 mV) than that with Nafion 212 (13 mV) with internal resistance of 10 Ω. In addition, The MFC with BPSH 40 produced about 10% higher maximum power density (126 mW m^{-2}) than that with Nafion 212 (111 mW m^{-2}).

1. Introduction

Microbial fuel cells (MFCs) convert chemical energy, available in a bio-convertible substrate, directly into electricity using bacteria as a catalyst. MFCs have a number of potential applications because they can harvest electricity in different types of wastewater. MFCs can use various kinds of waste and wastewater as a power source, including domestic and industrial wastewater and sludge in the anode compartment, and be used to conduct denitrification, or the removal of heavy metals in the cathode compartment. Moreover, MFCs can produce hydrogen, methane, or other valuable chemicals, and then become a microbial desalination cell for bio-electrochemical desalination using electrical energy [1].

The generation of electrical energy in MFC systems is significantly limited by the properties of the individual components such as electrodes, electrolytes and PEM. To achieve high voltage and power density, it is essential to optimize factors which can lower internal resistance in MFC. For example, highly exoelectrogenic activated bacteria, highly conductive electrodes with high surface area and high proton-conductive cation exchange membranes could greatly improve the power density of MFC [2]. Table 1 summarizes the maximum power densities obtained in various MFC systems using *Shewanella* species as bacteria. The MFCs exhibit a wide variety of power densities (6–1300 mW m^{-2}). In many cases, studies have been done to improve the electrochemical cell performance of MFC by reactor configurations, modifying the electrodes and varying the electrolytes (electron acceptor).

* Corresponding author. Tel.: +82 2 2220 2338; fax: +82 2 2282 0922.
E-mail address: badtzhb@hanyang.ac.kr (H.B. Park).

0378-7753/$ – see front matter © 2012 Elsevier B.V. All rights reserved.
http://dx.doi.org/10.1016/j.jpowsour.2012.07.109

Table 1
Maximum power density of MFC using Shewanella.

Reactor type	Anode	Cathode	Membrane	Electrolyte	Maximum power density (mWm^{-2})	Ref.
Two-chamber	Stainless steel	Graphite block	AEM-PES	Potassium permanganate (catholyte)	116.2	[36]
Two-chamber	Graphite felt	Graphite felt	Nafion 424	Sodium phosphate (both)	6	[37]
Two-chamber	Graphite felt	Graphite felt	Nafion 117	PIPES (both)	16	[37]
Two-chamber	Carbon paper	Carbon paper	Nafion	Humic acids (anode) 0.1 M potassium hexacyanoferrate (cathode)	100	[38]
Two-chamber	PPy/AQDS modified carbon felt	PPy/AQDS modified carbon felt	CEM	0.1 M PBS	1300	[39]
Two-chamber	Unmodified carbon felt	Unmodified carbon felt	CEM	0.1 M PBS	100	[39]
Two-chamber	Graphite felt	Carbon paper with Pt	Nafion 212	0.1 M PBS	100	This study
Two-chamber	Carbon paper treated ammonia	Carbon paper	Nafion 117	N/A	41	[40]
Single-chamber (H-type)	Carbon brush treated ammonia	Air cathode	Carbon cloth with PFTE and Pt	Air	332	[40]
Single-chamber (cubic)	Carbon brush treated ammonia	Air cathode	Carbon cloth with PFTE and Pt	Air	148	[40]
Single-chamber (cubic)	Graphite felt	Air cathode	BPSH 40	Air	126	This study
Single-chamber	Gold	Air cathode	Nafion with Pt/C	Air	29	[41]
Single-chamber	Graphite felt	Air cathode	PTFE with Pt	Air	68	[42]
Single-chamber	Graphite plate	Air cathode	Nafion with carbon cloth/Pt	Air	117	[43]

Polymer electrolyte membranes (or proton exchange membranes) (PEMs) physically separate the anode and cathode chamber, while allowing protons to transport from the anode to the cathode to maintain ion and electron balance [3]. Therefore, PEMs suitable for MFC are certainly necessary to improve MFC performance since the proton conductivity is a significant factor to accelerate electrochemical reaction kinetics in MFC [4]. Up to this time, Nafion has been frequently used as a PEM because it is the only commercially available PEM. In general, Nafion have many desirable properties such as high proton conductivity, excellent mechanical and thermal stability in various fuel cells such as polymer electrolyte membrane fuel cells (PEMFC) and direct methanol fuel cells (DMFC). However, the current densities in MFCs, to date, are 10^3–10^4 times lower than those in PEMFC [5]. Besides, there are several drawbacks such as high salt passage, undesirable electrolyte cross-over and high cost [6] e.g., about 38% of the capital costs in MFCs [7]. Salt passage and electrolyte cross-over through Nafion cause a significant loss of electrochemical cell performance in the cathode [8]. The high cost of Nafion is also a barrier for extensive use. In particular, there were no studies about chemical degradation of PEM in harsh MFC environments for its reliability in long term operations. Aqueous environments in MFC will provide operation conditions different from other fuel cells. As a result, new PEM materials have been sought for MFC applications. However, there are only a few studies about the effect of different types of PEMs on the electrochemical cell performance in MFC. Therefore, new materials need to be developed to make a step forward towards practical implementation of MFCs. Here, hydrocarbon based PEM, disulfonated poly (arylene ether sulfone) (BPSH), is considered an alternative PEM having high proton conductivity and good physical properties comparable with Nafion [9–11]. In addition, BPSH would be cheaper than Nafion [12], which can reduce the capital costs of MFC systems.

In this research, different types of PEMs that have not been previously evaluated for MFC applications were studied. Using a two-chamber and a single-chamber MFCs the performance of BPSH membranes was compared with that of Nafion membrane. The influence of PEMs on the cell performance of MFCs was further discussed.

2. Experimental sections

2.1. Synthesis of disulfonated poly(arylene ether sulfone) membranes

4,4′-Dichlorodiphenlysulfone (DCDPS) and 4,4′-biphenyl (BP) were purified with ethanol. 3,3′-Disulfonated-4,4′-dichlorodiphenylsulfone (SDCDPS) was synthesized according to the literature [13]. Then, DCDPS, BP, SDCDPS and potassium carbonate were added in a three-neck flask equipped with a mechanical stirrer, a nitrogen inlet and a Dean-stark trap. *N*,*N*-dimethylacetamide (DMAc, Aldrich) and toluene (Aldrich) were used as a solvent and an azeotrope agent. The reaction mixture was refluxed at 150 °C for 4 h to remove water and then the temperature was raised to 165 °C. The reaction was kept for 20 h, and the viscous solution was precipitated in an isopropyl alcohol and water mixture. The precipitated polymer was washed with water and dried in a vacuum oven at 120 °C for 24 h. The dried polymer was dissolved in DMAc and cast onto a glass plate. The cast polymer solution was dried at 60 °C for 24 h, and then vacuum-dried at 120 °C for 6 h. Membrane was delaminated from a glass plate by immersing in deionized water, and finally acidified with a boiling 1 M sulfuric acid [9] solution and then completely rinsed with deionized water to remove excessive acid.

2.2. Membrane characterizations

2.2.1. Ion exchange capacity (IEC) & proton conductivity

IEC was determined *via* the titration of the released amount of H^+ of the polymer in an acid form in 1 M NaCl with 0.1 M NaOH by using phenolphthalein as an indicator. The IEC values (meq g^{-1}) were obtained from the following equation:

$$\mathrm{IEC} = \frac{V_{\mathrm{NaOH}} C_{\mathrm{NaOH}}}{W_{\mathrm{dry}}} \quad (1)$$

where V_{NaOH} is the volume of NaOH (mL) to use titration, C_{NaOH} is the concentration of NaOH (mM), and W_{dry} (g) in the weight of dried membrane [14].

The proton conductivity was measured using the four-point probe technique in the water at 30 °C. Each sample was cut in 4×1 cm^2 prior to mounting on the cell. The proton conductivity (σ) was obtained from the following equation:

$$\sigma = \frac{l}{RS} \quad (2)$$

where σ is the proton conductivity (S cm^{-1}), and l is the distance between the electrodes used to measure the potential (cm). R is the impedance of the membrane (Ω) and S is the cross-sectional area of the membrane (cm^2) [15].

2.2.2. Water content, dimensional change and mechanical strength

The water uptake absorbed in the membranes was measured by immersing the membranes sample into the deionized water at 30 °C for 24 h [16]. The weight of the swollen membranes was measured after removing excessive water drops on the surface. The water content, W, was calculated from the following equation:

$$\text{Water uptake}(\%) = \frac{W_{\text{wet}} - W_{\text{dry}}}{W_{\text{dry}}} \times 100 \quad (3)$$

where W_{dry} and W_{wet} are the weight of the dried and the swollen membrane, respectively.

The dimensional change (%) was evaluated by measuring the change in sample size through an optical microscope (SV-35, Sometech, Seoul, Korea) before and after immersing. The ratio of the volume of swollen (V_{wet}) and dried (V_{dry}) membrane was calculated from the following equation.

$$\text{Dimensional change}(\%) = \frac{V_{\text{wet}} - V_{\text{dry}}}{V_{\text{dry}}} \times 100 \quad (4)$$

The mechanical strength of membrane was measured using an INSTRON-1708 (Boston, MA, US) and analyzed according to the ASTM D882 standard test protocol for thin film tensile tests [17].

2.2.3. Salt permeability

Salt transport measurement was conducted using a two-chambered diffusion cell. One compartment (40 mL) was filled with 171 mM sodium chloride (NaCl) solution, and the other compartment was filled with deionized water. Effective membrane area was 0.785 cm^2 ($\Phi = 1$ cm). The conductivity rise in a chamber filled with deionized water was measured by a conductivity meter (LR 325/01, WTW, Germany) as a function of time, and calculated and converted by terms of salt permeability with the following equation:

$$Pt = \ln\left[1 - 2\frac{C_R(t)}{C_D(0)}\right]\left[-\frac{Vd}{2A}\right] \quad (5)$$

where P is salt permeability (cm^2 s^{-1}), t is measurement time (s), C_R is concentration of receiver (mM), C_D is concentration of donor (mM) ($C_D << C_R$ during the entire experiment, C_D is essentially constant during the experiment), V is reactor volume (mL), d is thickness of membrane (μm) and A is area of membrane (cm^2).

2.3. Microbial inoculation

Shewanella putrefaciens was obtained from Korean Collection for Type Culture (KCTC). *S. putrefaciens* was maintained aerobically on LB agar (Difco™ LB Agar, Miller, USA). Inoculum was cultivated aerobically in LB liquid medium (Difco™ LB Broth, Miller, USA) at 30 °C with shaking at a rate of 200 rpm. The concentration of cells was estimated by measuring optical density at 600 nm (OD_{600}). The culture was adjusted to an OD_{600} of 0.5 and 200 mL was inoculated into the anode chamber [18–20].

2.4. MFC configurations

A two-chamber MFC reactor was installed using two-cylindrical glass chambers (225 mL) equipped with feed inlet and outlet, gas inlet and outlet and electrode connection parts (Fig. 1). Carbon paper (TGPH-090, Toray Inc., Japan) or graphite felt electrodes (Morgan, Saint Mary's, PA, USA) were used as anode materials. The effective surface area of electrode held by a PTFE frame was 4 cm^2. The anode chamber was purged with N_2 to maintain continual anaerobic condition. Pt-coated (10 wt. %) carbon paper (FCearth, USA) clamped by a PTFE holder was used as a cathode material. The cathode chamber was supplied with oxygen as an electron acceptor through the aeration. The chambers were divided by PEMs with an active area of 7 cm^2. The design of the single cell MFC was based on a cubic-shaped MFC, whose chamber was fabricated by drilling a hole in a solid block of polycarbonate (PC). A graphite felt was used as an anode, whereas the cathode was prepared in the form of MEA (membrane–electrode-assembly) prepared by hot-pressing PEMs (BPSH or Nafion) between Pt-coated (10 wt. %) carbon cloths (FCearth, USA). Anolyte was used LB broth (25 g L^{-1}) which was adjusted the pH 7.3 with 0.1 M PBS and 1 N NaCl, and catholyte was used 0.1 M PBS which was adjusted the pH 7.3. The effective surface area of the electrode was about 11 cm^2. In a continuous feeding-flow mode, a feed flow rate was controlled by a peristaltic pump (Longer, China).

2.5. Scanning electron microscopy (SEM)

The surface morphologies of membranes were characterized using a SEM (JSM-7600F, JEOL, Japan). Microbial grown on the electrode and membrane surfaces were fixed in 4% glutaraldehyde solution for more than 4 h. After washing three times in a PBS solution (pH 7.0), the samples were dehydrated in ethanol solution series (50%, 60%, 70%, 80%, 90% and 95%) for each 10 min and then rinsed twice in 100% ethanol for 10 min. The samples were substituted by isoamyl acetate and hexamethyldisilazane (HMDS) and then dried in the air [21].

2.6. Confocal laser scanning microscopy (CLSM)

The biofilms on the membrane surfaces were stained with bacterial viability kit (L7012, Live/Dead BacLight Bacterial viability kit, for microscopy, Invitrogen, USA). The stained biofilms were observed using a confocal laser scanning microscopy (CLSM, Eclipse 90i, Nikon, Japan) equipped with an argon-krypton laser and Bio-Rad Radiance scanning confocal system. The CLSM images were reconstructed using a digital images analysis program (IMARIS, ver. 6.1.5, Bitplane AG, Zurich, Switzerland) [22].

2.7. Electrochemical performance measurements

The voltage (V) across the external resistor (10 Ω) was monitored at 30 s interval using Datalogger (34972A, Agilent, USA) connected to a personal computer and converted to current and power according to $V = IR$ and $P = IV$. Current density (A m^{-2}) and power density (W m^{-2}) were calculated by normalizing current and power to the anode surface area [23]. The linear sweep voltammetry (LSV) was performed at a scan rate of 1 mV s^{-1} in a range from an open circuit voltage (OCV) to +0.2 V using a workstation (Zive SP2, Wonatech, Korea). The cyclic voltammetry (CV) were performed in the range from −0.8 to +0.6 V vs. Ag/AgCl at a scan rate of 1 mV s^{-1} with the same workstation. Anode and cathode

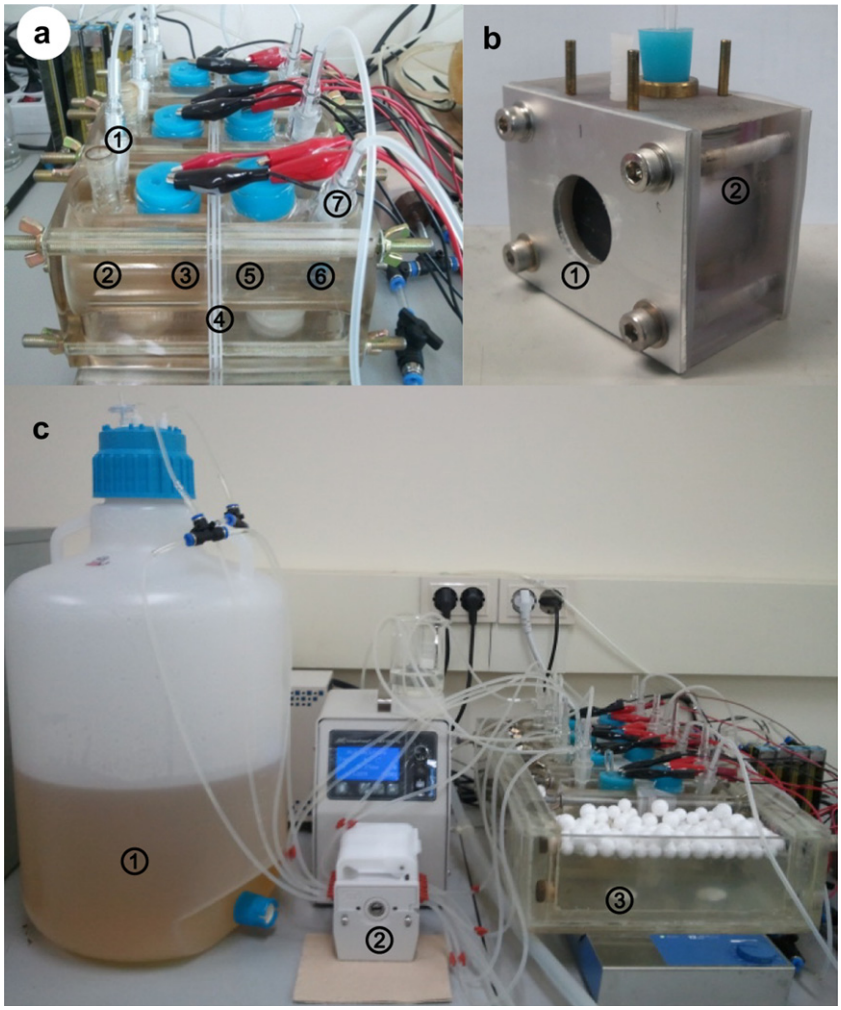

Fig. 1. Current MFC system: (a) two-chamber (① N_2 purge, ② anolyte: LB broth (25gL^{-1}), ③ anode (4 cm^2): carbon paper and graphite felt, ④ membrane: 7 cm^2, ⑤ cathode (4 cm^2): carbon paper (10 wt.% Pt), ⑥ catholyte: 0.1 M PBS (200mL), ⑦ aeration), (b) single-chamber (① cathode (MEA), ② anode: graphite felt) and (c) continuous feeding system (① feed: LB broth (25gL^{-1}), ② feed rate: 1 Lday^{-1}, ③ temp.: 30°).

electrodes were used as working and counter electrodes, respectively. The reference electrode was an Ag/AgCl (KCl-sat.) electrode [6,24].

3. Results and discussion

3.1. Effect of the degree of sulfonation on IEC and proton conductivity

PEMs need positively charged mobile ions available for salt ion exchange. This functional group determines the electrode chemical behavior of the membrane. PEMs in MFC are highly ionized in the acid form ($R-SO_3^- H^+$) of the sulfonic acid group. The effect of the degree of sulfonation (DS) on the ion exchange capacity (IEC) of BPSH membranes are summarized in Table 2. The IEC of BPSH membranes depends on the DS, it increases with the increase of DS. BPSH 40 and 60 membranes show higher IEC values than that in Nafion 212.

Proton conductivity is one of important electrochemical factors determining MFC performance. Proton conductivity of BPSH membranes is proportional to DS, which is in accordance with the effect of DS on IEC. As compared with Nafion 212, BPSH

Table 2
Physical properties of BPSH series and Nafion 212.

	IEC (meq/g)	Proton conductivity (S cm^{-1})	Salt (NaCl) permeability (cm^2 s^{-1})	Water uptake (wt. %)	Dimensional change (%)	Elongation at break (%)		Tensile strength (MPa)	
						Before	After 7 days	Before	After 7 days
Nafion212	0.93	0.118	9.0×10^{-10}	11.6	8.7	254.2	122.3	24.5	28.9
BPSH 20	1.00	0.039	6.2×10^{-11}	14.0	6.9	92.6	63.0	49.0	44.7
BPSH 30	1.34	0.066	2.9×10^{-10}	21.2	7.4	76.6	21.9	23.7	23.0
BPSH 40	1.82	0.144	2.2×10^{-9}	33.3	16.9	98.1	68.4	44.8	49.2
BPSH 60	2.21	0.186	5.6×10^{-8}	160.0	55.9	111.6	11.5	22.3	22.1

40 and 60 membranes showed higher proton conductivities. However, BPSH 20 and 30 exhibited much lower proton conductivities than Nafion 212, although these membranes have similar or more sulfonic acid groups. Nafion 212 shows a much higher conductivity than BPSH membranes even though it has less ionized functional groups on a mass basis. When a proton is transported through PEM in an aqueous media system, it is conducted in the form of hydrated ion. Therefore, the water molecules through the ionic domain of each membrane may affect the proton conductivity. The water diffusion through the PEMs can be strongly affected by the morphological structure of the ion domains. Fig. 2 shows the chemical structures of Nafion and BPSH membranes. Nafion, the sulfonic acid group is located at the end of a long and flexible perfluoroether side chain whereas the sulfonic acid group of BPSH is directly connected to the aromatic backbone. Therefore, hydrophilic domain formation of Nafion is more facile because of long, flexible side chains than that of BPSH. As a result, Nafion showed higher proton conductivity than BPSH membranes in spite of low sulfonic acid group concentration [25].

3.2. Effect of the degree of sulfonation on water uptake & dimensional change

Water uptake is a significant property to evaluate the performance of PEM. In a certain level, water molecules are essential to transport protons through the membrane as mentioned above. In general, water content is increased with higher DS because sulfonic acid groups generate enough hydrophilic ionic domains to absorb more water molecules. Table 2 lists the water uptake properties of Nafion and BPSH membranes. In particular, the water uptake of BPSH 60 is much higher than those of other PEMs. However, the highest water content negatively affected the mechanical strengths of PEMs by excessive swelling. Table 2 also summarizes the dimensional change of PEMs by increasing DS in BPSH series. As expected, BPSH 60 has a much higher dimensional change than other PEMs. As the dimensional change in PEM increases, the polymeric matrix is getting looser and makes larger spaces between polymer chains. As a result, it can transport not only protons, but also other undesirable cations and small molecules in the electrolyte through the PEM. Therefore, the control of water uptake would be critical to reduce the adverse effects by swelling and losing the mechanical strengths of the membrane in such an aqueous system [26].

3.3. Salts transport & electrolyte cross-over through PEMs

Typically the concentration of other salts is 10^5 times higher than proton concentrations in a MFC system with wastewater at pH neutral conditions [5]. The LB-broth media solution also contains a large amount of salt ions which are essential to grow bacteria. Among them, the concentration of sodium chloride is about 171 mM that is the highest concentration in the media solution. Table 2 shows NaCl permeability through PEMs in the water. With the increase of the DS, both proton conductivity and NaCl permeability increase. The increase of NaCl permeability will inevitably result in the transport of NaCl in anolyte through PEM and the increase of NaCl concentration in catholyte. Transport of salt ions through the membrane interrupts proton transport so that electrochemical cell performance in MFC will be decreased. Cross-over of electrolytes, except water molecules, through the loosen PEM matrix causes various side reactions in cathode compartment.

Fig. 3(c) shows the current density change in a batch mode MFC using carbon paper electrode. MFC installed with BPSH 60 membrane showed a significantly lower performance whereas other MFCs with different PEMs exhibited much higher performance. In Fig. 3(a) and (b), the catholyte of MFC using BPSH 60 membrane was contaminated by an anolyte cross-over through the membrane, and the solution color was changed from transparent to opaque whereas that of MFC using Nafion 212 membrane still showed transparent catholyte. These results indicate that electrolyte cross-over has a significant effect on MFC cell performance. BPSH 60 membrane showed the highest water uptake and dimensional change which causes its polymer matrix to loosen. It was caused by cross-over of any chemicals in anolyte to cathode compartment, and led to the side reactions in catholyte, resulting in reducing cell performance of MFC. There are several main factors affecting electrolyte cross-over through the PEM between anode and cathode compartments. One in particular, the cross-over of other salt ions caused by the difference in ion concentration, also significantly affects the proton transport and causes side reactions in catholyte, leading to a decrease in electrochemical potential of MFC cell. Secondly, severe swelling in PEMs also impacts on

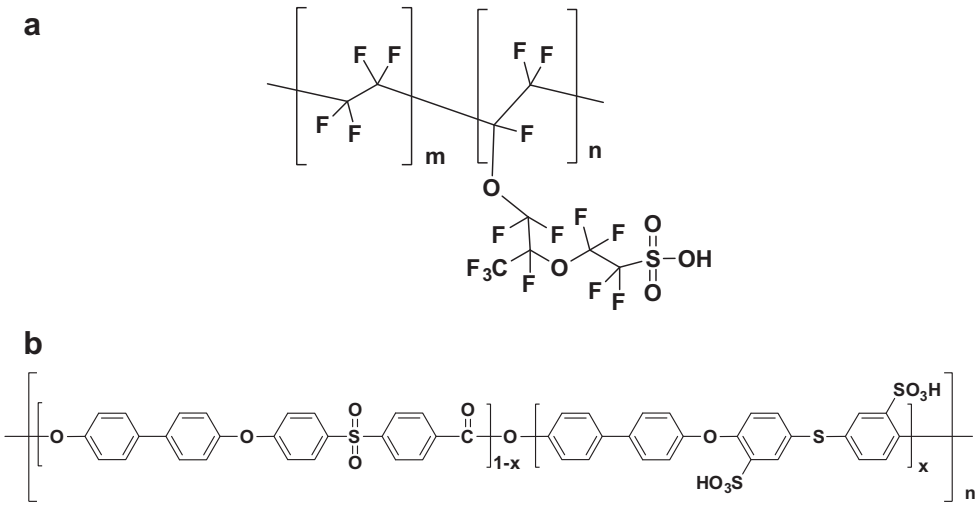

Fig. 2. Chemical structures of (a) Nafion and (b) BPSH.

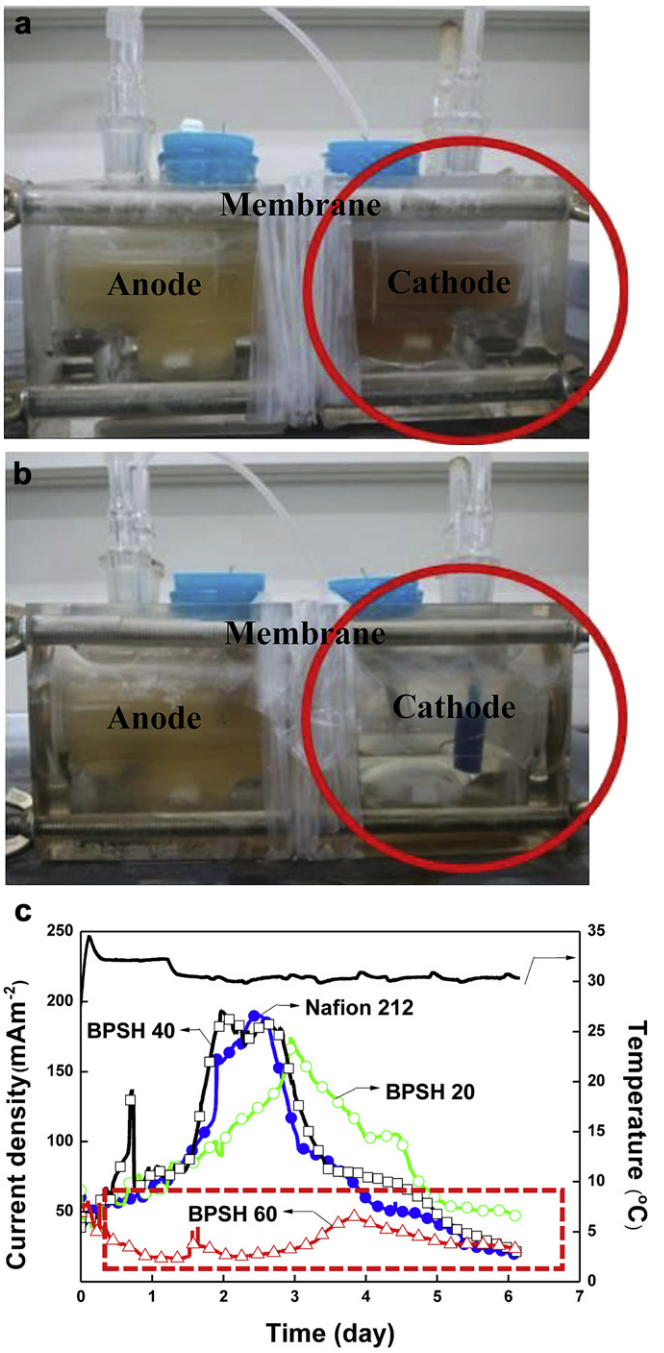

Fig. 3. Electrolyte cross-over through (a) Nafion 212, (b) BPSH 60, and (c) current-density decline of BPSH 60.

electrolyte cross-over through the polymer matrix. The amount of electrolyte cross-over could vary by the degree of swelling in PEMs even though each MFC system has the same osmotic pressure and different concentrations. Furthermore, osmotic pressure between anolyte and catholyte may hinder the proton transport from anode chamber to cathode chamber.

3.4. Bio-fouling on the surface of polymer electrolyte membrane

Different from biofilm formation on the electrode, bacteria clusters on the membrane surface may cause bio-fouling, leading to preventing effective proton transport through the PEMs. Bio-

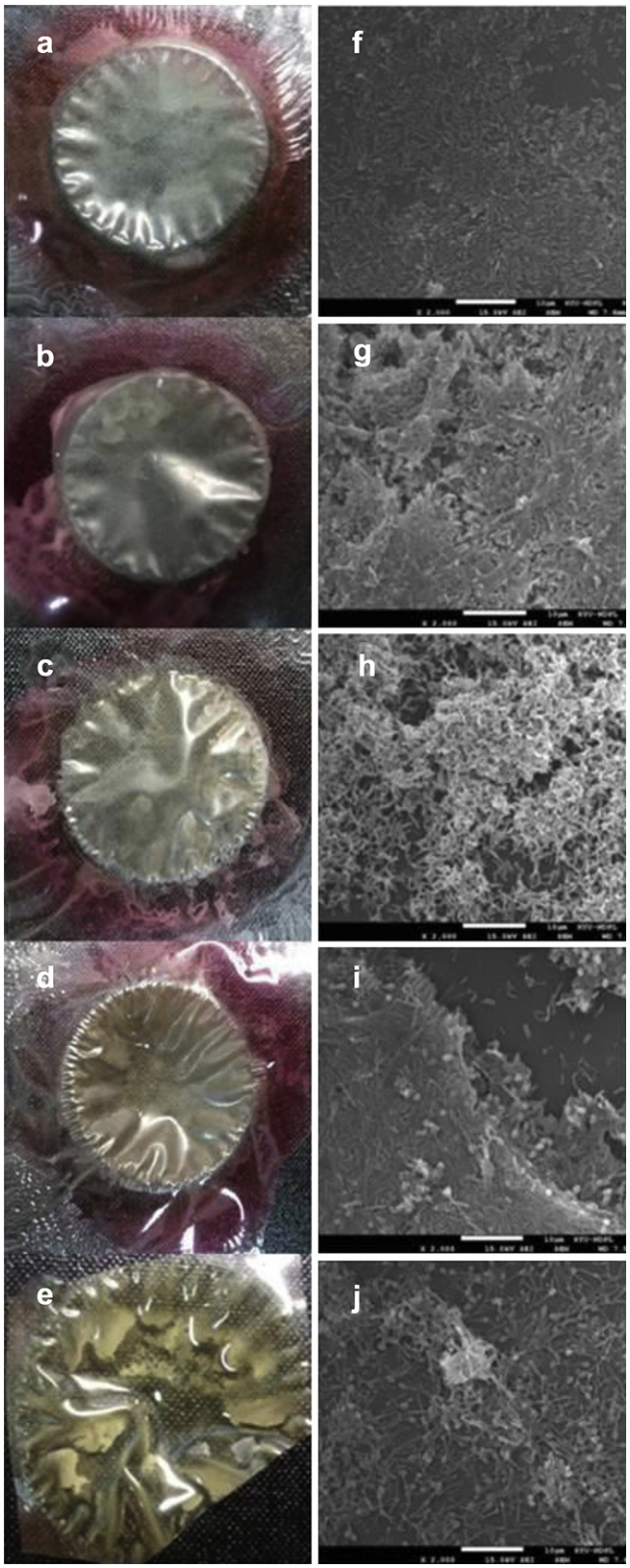

Fig. 4. Bio-fouling on the surface of PEMs: (a) Nafion 212, (b) BPSH 20, (c) BPSH 30, (d) BPSH 40, (e) BPSH 60 and SEM micrographs: (f) Nafion 212, (g) BPSH 20, (h) BPSH 30, (i) BPSH 40, (j) BPSH 60.

foulings are due to organic foulants such as extracellular polymeric substances (EPS) and soluble microbial products (SMP) participating in bacteria aggregation and clusters (Fig. 4(f)–(j)). Besides, the large amount of salt ions in the media solution also increases the electrical resistance of PEM by irreversible fouling [3]. Cations can lead to the intermolecular bridging between biofoulants and the fouling layer [27]. Hence, these bacteria, biofoulants and cations can form dense biofilms on the surface of the PEMs to cause higher electrical resistance. Fig. 4 shows the bio-fouling on the surface of Nafion and BPSH membranes. Fouling can be classified into reversible fouling and irreversible fouling irrespective of physical cleaning. Reversible bio-fouling can be removed easily by washing and brushing. However, irreversible bio-fouling can strongly affect physical and chemical properties of membranes such as proton conductivity, degradation and elongation etc. As listed in Table 2, the mechanical strengths of Nafion and BPSH membranes were measured before MFC operation and after 7 days. Elongations at break in all PEMs were reduced after 7 days while tensile strengths in all PEMs have little change before and after. Particularly Nafion 212 and BPSH 60 membranes showed huge differences in elongation at break. It suggests that PEMs after MFC operation becomes more brittle than before, and these changes in mechanical strength affect the durability of PEM during MFC operation for a long period.

The relationship between bio-fouling and hydrophilicity in the membrane surface has been demonstrated according to membrane areas, particularly in-water treatment membrane processes. Fig. 5 shows the effect of hydrophilicity to DS on bio-fouling. Bio-film was formed on the membrane surface of PEM though a Center for Disease Control (CDC) reactor for two days and then observed using CLSM. A large amount of bacterial cluster formed on the surface of BPSH 20 membrane (Fig. 5(b)). On the other hand, bio-film rarely formed on the surface of BPSH 60 membrane (Fig. 5(e)). With increasing hydrophilicity in membrane by DS, the amount of bio-film formed on the surface to the PEMs decreased. However, once a membrane was fouled, bio-film was formed easily independent of membrane hydrophilicity. Therefore, further study would be necessary to evaluate the relationship between bio-fouling and hydrophilicity in the long term.

3.5. Two-chamber MFC performance in a continuous feeding system

Voltage changes in the MFC with different membranes as a function time are shown in Fig. 6. For about 15 h the voltages of all MFCs increased rapidly, and reached the maximum value. It is directly related to the growth curve of *S. putrefaciens*. *S. putrefaciens* generally shows fast growth activity for early 15 h, and then the growth curve was stabilized. Initial voltage curves were similar to the growth curve of Shewanella. It supports that initial voltage change in MFC strongly depends on microbial growth and its bio-film formation. In MFC with BPSH 40, the maximum voltage reached 12.1 mV after 12 h. In the case of Nafion 212, the maximum voltage reached 11.6 mV after 16 h, and the maximum voltages of MFCs with BPSH 30 and 20 reached 10.1 mV and 9.7 mV after 22 h, respectively while MFC with BPSH 40 reached at the highest maximum voltage in the shortest time. The remarkable increase of voltage at the beginning of MFC operation is related to the proton conductivity of PEM. The cell voltage increased faster as the PEM of the cell with higher proton conductivity (Table 2). It indicates that the initial performance of MFC is strongly influenced by the proton conductivity in PEM.

However, voltages declined in all MFCs after maximum voltage, in spite of the continuous feeding mode. After 36 h, voltage in MFC with BPSH 40 deceased 4.3 mV (from 12.1 mV to 7.8 mV) and the voltages in MFC with Nafion 212, BPSH 30 and BPSH 20 deceased 3.9 mV (from 11.6 mV to 7.7 mV), 3.3 mV (from

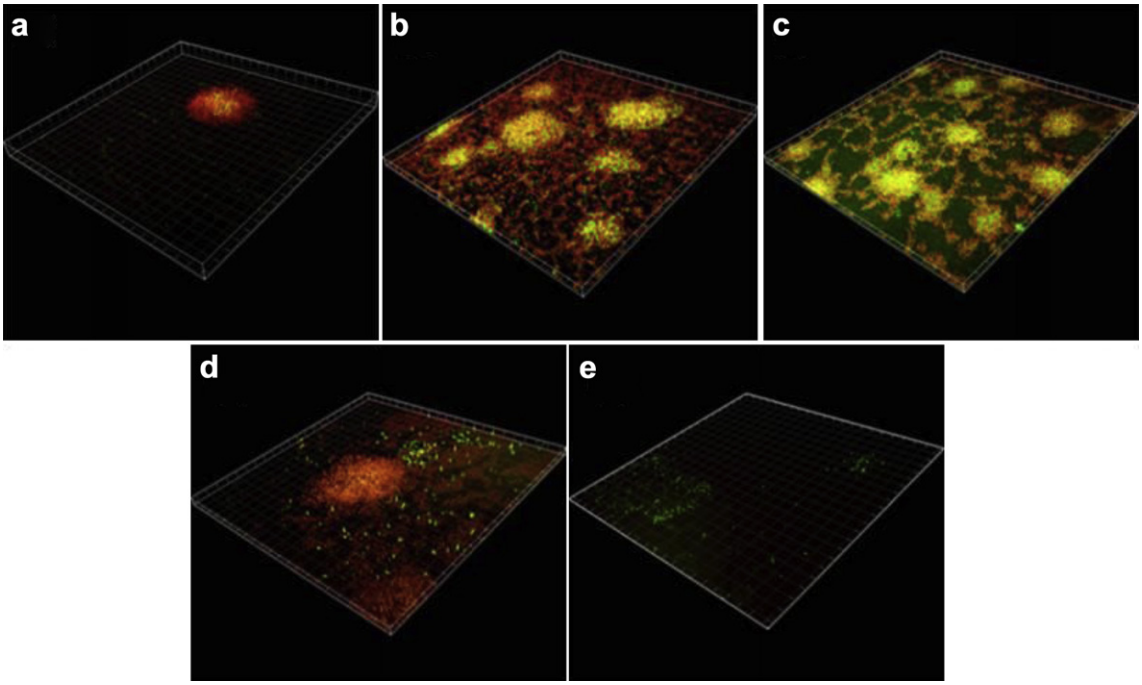

Fig. 5. Effect of surface hydrophilicity on bio-fouling: (a) Nafion 212, (b) BPSH 20, (c) BPSH 30, (d) BPSH 40 and (e) BPSH 60 observed using a confocal laser scanning microscopy (CLSM).

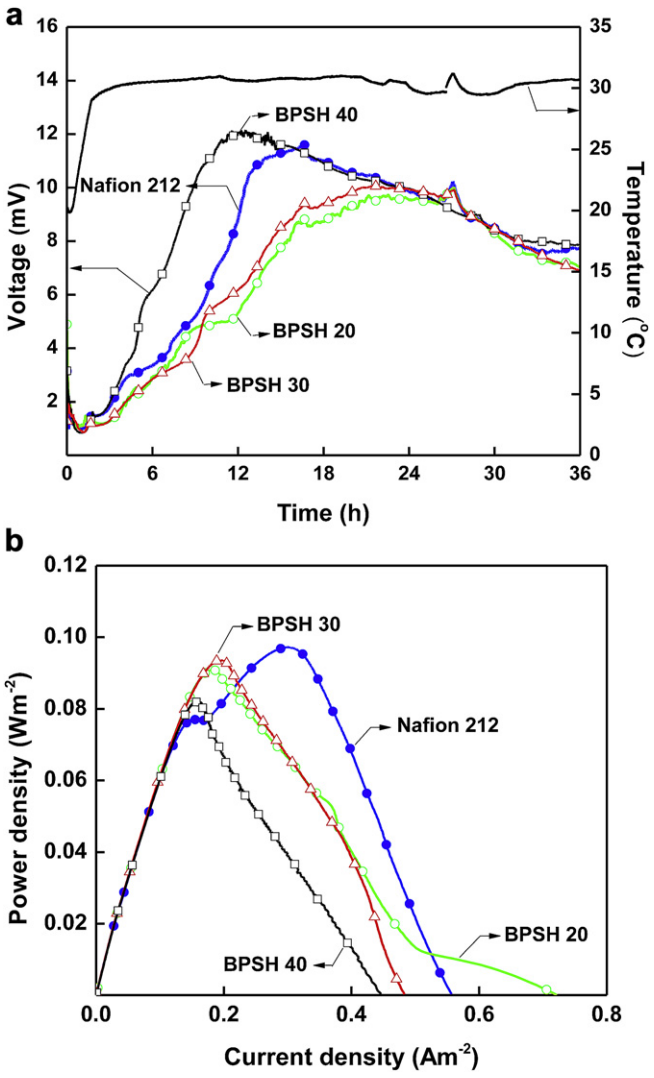

Fig. 6. (a) Voltage change (with external resistance of 10 Ω) and (b) power density of two-chamber MFCs based Nafion 212 (blue circle) and BPSH series (open green circle: BPSH 20, open red triangle: BPSH 30, open black square: BPSH 40) in a continuous system. (For interpretation of the references to colour in this figure legend, the reader is referred to the web version of this article.)

10.1 mV to 6.8 mV), 2.7 mV (from 9.7 mV to 7.0 mV). In the case of BPSH 60, the degree of voltage decline was the largest. It is similar to the tendency in NaCl permeability (Table 2), that is, the voltage decline might be related to the changes of electrolyte and PEMs. With increasing transport of many cations including NaCl from anode chamber to cathode chamber through PEM, proton transport decreases relatively. As a result, an activity of electrochemical reaction such as oxygen reduction reaction may be reduced, and the cell performance of MFC might also be decreased. The anode media solution contains many types of cations to be related to microbial metabolism, so these cations occupy the negatively charged sulfonic acid groups being able to transport protons through the PEMs [3,28]. As a result, the proton conductivity of the salt formed PEMs decreased, and the performance of MFC might also be reduced.

Current-voltage characteristic (I–V curve) is shown in Fig. 7(a). As compared with typical polarization curve of fuel cell [29], the large amount of ohmic losses were in the MFC system. There are several main factors such as distance between electrodes, resistances of electrode and membrane materials, electrolyte conductivity and so on. Amongst them, the resistance of catholyte, specially, in a two-chamber MFC system plays an important role in determining power output. In Fig. 6, the maximum power density of MFC with Nafion 212 was 100 mW m^{-2}, and those of BPSH 30, BPSH 20 and BPSH 40 were 93 mW m^{-2}, 91 mW m^{-2} and 82 mW m^{-2}, respectively. The maximum power density of BPSH 20 was similar to those of Nafion 212 and BPSH 30 in spite of low proton conductivity, whereas BPSH 40 showed the lowest power density despite high proton conductivity. These results indicate that the change of catholyte by cations transport and electrolyte cross-over through PEM affect bacteria metabolism and electrochemical reactions on electrodes, and thus the cell performance of MFC. The fact is supported by current–voltage characteristics of anode and cathode as shown in Fig. 7 (b) and (c). In Fig. 7(b), the current density of BPSH 20 was similar to that of BPSH 40, but lower than those of Nafion 212 and BPSH 30. However, the results of overall system are somewhat different; BPSH 20 exhibited almost the same current density as BPSH 30, and higher than BPSH 40 (Fig. 7(a)). Although the anode reaction is a key step to determine overall cell performance in terms of kinetics rate since the current density of anode is much lower than that of cathode, the cathode reaction in catholyte also needs to be considered. In Fig. 7(c), BPSH 20 showed much higher electrochemical performance than other PEMs in the cathode side, as a result, increasing the current density in overall system in the case of BPSH 20. These electrochemical reactions in the catholyte might be strongly influenced by PEM properties such as electrolyte cross-over due to swelling, proton conductivities, and the oxygen reduction reaction (ORR) in the cathode side.

In cyclic voltammetry (CV), the MFC with BPSH 20 also showed the strongest activity, the highest peak, whereas the MFC with BPSH 40 exhibited reduced electrochemical activities, and the lowest peaks. Each peak indicates the presence of some redox species in *Shewanella* (Fig. 8). In general, the primary electron transfer process (cytochromes, other redox proteins, tethered electron shuttles and so on) happens in the range of −0.45 to −0.2 V (vs. Ag/AgCl) [30]. In some studies [31], under anaerobic and aerobic conditions electrochemical activities of *S. putrefaciens* and *E. coli* were measured through CV. Anaerobically grown *S. putrefaciens* was electrochemically active. It contains a redox potential of around −0.2 V (vs. Ag/AgCl) in CV curve [32]. It is plausible that the electrochemical activity is due to the cytochromes on the cell surface, with the orientation of the electrochemically active heme group toward the cell surface [33]. Electrochemical activity was observed in neither *S. putrefaciens* grown under aerobic condition, nor the *E. coli* in that study. In our MFC system, the detected peak at −0.4 V (vs. Ag/AgCl) also showed the presence of extracellular flavins in *Shewanella* grown anaerobically as shown in some studies that the primary mediators excreted by Shewanella are riboflavin and flavin mononucleotide (FMN) [30,34]. Other peaks between −0.3 and −0.2 V (vs. Ag/AgCl) also showed the existence of a second redox species not yet characterized [35].

3.6. Single-chamber MFC performance in a continuous system

The effect of PEMs on the performance of a single-chamber MFC was also examined in continuous system. As shown in Fig. 9, voltage generation and power density of MFC were significantly affected by the PEM. While the MFC with Nafion 212 generated a voltage of 15 mV, MFC with BPSH 40 generated a voltage of 20 mV. The voltage generation of MFC with BPSH 40

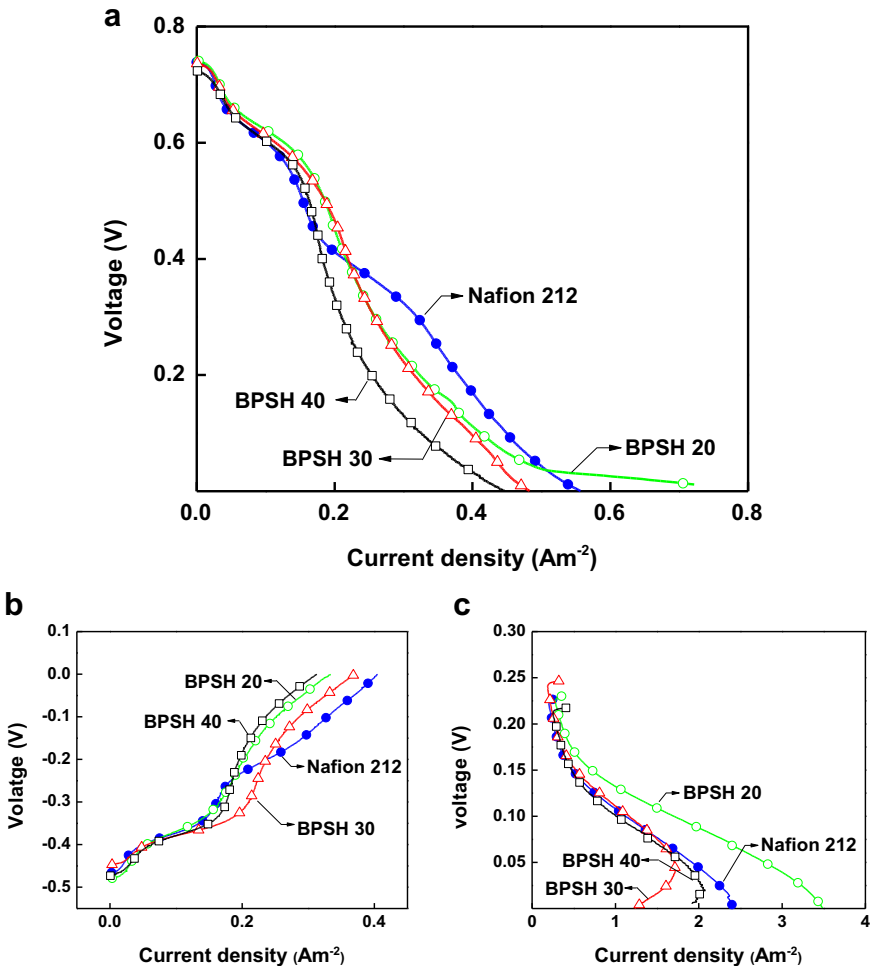

Fig. 7. *I–V* curve of (a) entire system, (b) anode and (c) cathode compartment (blue circle: Nafion 212, open green circle: BPSH 20, open red triangle: BPSH 30, open black square: BPSH 40) with a scan rate of 1 mV s^{-1}. (For interpretation of the references to colour in this figure legend, the reader is referred to the web version of this article.)

was almost 30% higher than that of MFC with Nafion 212 (Fig. 9(a)). In addition, at a current density of 0.6214 A m^{-2}, the MFC with BPSH 40 had maximum power density (126 mW m^{-2}) that was almost 10% higher than that of the MFC with Nafion 212

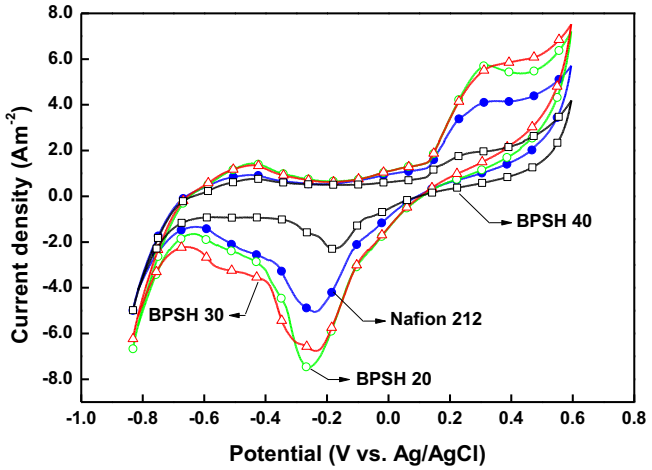

Fig. 8. Cyclic voltammetry of MFCs based Nafion 212 (blue circle) and BPSH series (open green circle: BPSH 20, open red triangle: BPSH 30, open black square: BPSH 40) with a scan rate of 1 mV s^{-1}. (For interpretation of the references to colour in this figure legend, the reader is referred to the web version of this article.)

(111 mW m^{-2}) (Fig. 9(b)). These results are dissimilar to those of two-chamber MFC that the performance of BPSH 40 is lower than that of Nafion 212. Overall, the performance of single-chamber MFC is significantly higher than that of two-chamber MFC. Particularly, maximum voltage generation of single-chamber MFC (20 mV) and maximum power density (126 mW m^{-2}) was increased almost 67% and 30%, compared with those of two-chamber MFC (12 mV, 100 mW m^{-2}). This is because the resistance of catholyte reaction is reduced. Above all, there are no electrolyte changes such as substance and salt loss through the PEM because catholyte in single-chamber MFC is not liquid. Furthermore, high proton conductivity of BPSH 40 is helpful to transfer more protons to oxygen directly than that of Nafion 212 in ORR. That suggests that the property of PEM and the status of catholyte play an important role in improving performance of MFC.

As shown in Fig. 10, however, high water uptake of BPSH 40 caused another problem like swelling of MEA so that contact between carbon cloth and membrane was weakened and internal resistance of MEA was increased. Like other hydrogen fuel cells, such as PEMFC, the MEA fabrication, adhesion between surfaces of electrode and membrane, is important factor in single-chamber MFC to transfer proton effectively. MEA detachment of BPSH 40 (Fig. 10(b)) can cause oxygen back diffusion to anode chamber through the loosen matrix of membrane as well as contact resistance.

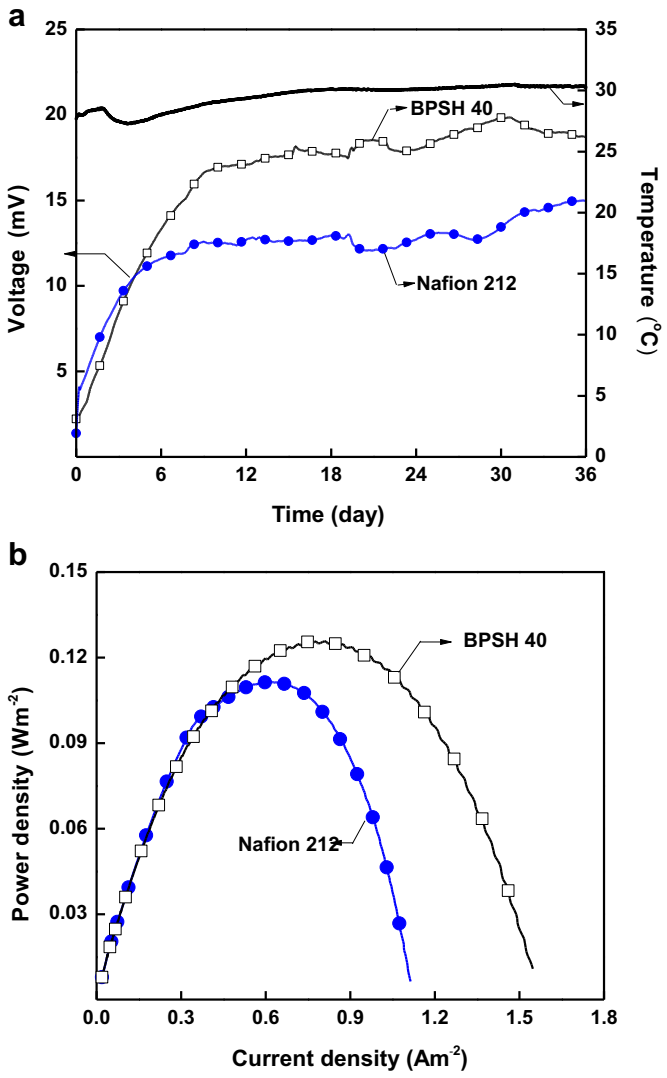

Fig. 9. (a) Voltage change (with external resistance of 10 Ω) and (b) power density of single-chamber MFCs based Nafion 212 (blue circle) and BPSH 40 (open black square) in a continuous system. (For interpretation of the references to colour in this figure legend, the reader is referred to the web version of this article.)

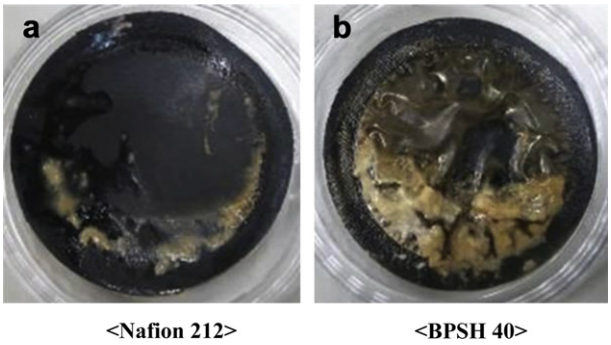

Fig. 10. Fouling and swelling of (a) Nafion 212 and (b) BPSH 40 in single-chamber MFC.

4. Conclusions

This study compared the electrochemical performance of MFC using Nafion 212 membrane and newly synthesized BPSH membranes with different degree of sulfonation. From membrane characterizations, it was found that the amount of sulfonic acid group in the BPSH membrane is important factor that determines the electrical efficiency of the membrane. The highly sulfonated BPSH (BPSH 40 and 60) showed higher conductivity, above 0.12 S cm^{-1} at 30 °C in the water, than Nafion 212. By increasing the hydrophilic ionic domain of the hydrocarbon based PEMs, the proton conductivity was increased. However, high water swelling property can cause critical problems such as high electrolyte cross-over and high cation transport and accumulation rather than protons. As a result, two-chamber MFCs with BPSH 20 and 30 showed greater performance than other PEMs in electrochemical measurements (*I–V* curve, power density and cyclic voltammetry) in spite of lower proton conductivity. However, single-chamber MFC with BPSH 40 showed greater performance than others compared with two-chamber MFC in spite of MEA swelling. In consideration of the overall cell performance, MFCs using hydrocarbon based PEM exhibited the same electrochemical performance as the Nafion based MFC, depending on the sulfonation degree. Therefore, further study is needed to determine the proper composition of hydrocarbon membrane, such as the ratio of hydrophilic and hydrophobic domains, and to improve MEA adhesion between electrode and membrane, especially in single-chamber MFC. The optimization of those factors can further improve the cell performance of MFCs.

Acknowledgment

This research was supported by WCU (World Class University) program through the National Research Foundation of Korea funded by the Ministry of Education, Science and Technology (R31-10092).

References

[1] F. Zhang, K.S. Brastad, Z. He, Environmental Science & Technology (2011).
[2] B.E. Logan, Microbial Fuel Cells, Wiley-Interscience, 2008.
[3] M.J. Choi, K.J. Chae, F.F. Ajayi, K.Y. Kim, H.W. Yu, C. Kim, I.S. Kim, Bioresource Technology 102 (2011) 298–303.
[4] K.J. Chae, M. Choi, F.F. Ajayi, W. Park, I.S. Chang, I.S. Kim, Energy & Fuels 22 (2007) 169–176.
[5] R.A. Rozendal, H.V.M. Hamelers, C.J.N. Buisman, Environmental Science & Technology 40 (2006) 5206–5211.
[6] Y. Zuo, S. Cheng, B.E. Logan, Environmental Science & Technology 42 (2008) 6967–6972.
[7] X. Tang, K. Guo, H. Li, Z. Du, J. Tian, Biochemical Engineering Journal 52 (2010) 194–198.
[8] B. Viswanathan, M. Helen, Bulletin of the Catalysis Society of India 6 (2007) 50–66.
[9] F. Wang, M. Hickner, Y.S. Kim, T.A. Zawodzinski, J.E. McGrath, Journal of Membrane Science 197 (2002) 231–242.
[10] Y.S. Kim, L. Dong, M.A. Hickner, B.S. Pivovar, J.E. McGrath, Polymer 44 (2003) 5729–5736.
[11] Y.S. Kim, M.A. Hickner, L. Dong, B.S. Pivovar, J.E. McGrath, Journal of Membrane Science 243 (2004) 317–326.
[12] C.W. James Jr., A. Roy, J.E. McGrath, E. Marand, Journal of Membrane Science 309 (2008) 141–145.
[13] M. Sankir, V. Bhanu, W. Harrison, H. Ghassemi, K. Wiles, T. Glass, A. Brink, M. Brink, J. McGrath, Journal of Applied Polymer Science 100 (2006) 4595–4602.
[14] D.S. Kim, H.B. Park, J.W. Rhim, Y.M. Lee, Solid State Ionics 176 (2005) 117–126.
[15] C.H. Lee, C.H. Park, Y.M. Lee, Journal of Membrane Science 313 (2008) 199–206.
[16] J.W. Rhim, H.B. Park, C.S. Lee, J.H. Jun, D.S. Kim, Y.M. Lee, Journal of Membrane Science 238 (2004) 143–151.
[17] D.S. Kim, H.B. Park, Y.M. Lee, Y.H. Park, J.W. Rhim, Journal of Applied Polymer Science 93 (2004) 209–218.
[18] D.P. Moser, K.H. Nealson, Applied and Environmental Microbiology 62 (1996) 2100.
[19] M. Sun, F. Zhang, Z.H. Tong, G.P. Sheng, Y.Z. Chen, Y. Zhao, Y.P. Chen, S.Y. Zhou, G. Liu, Y.C. Tian, Biosensors and Bioelectronics 26 (2010) 338–343.
[20] O. Bretschger, A. Obraztsova, C.A. Sturm, I.S. Chang, Y.A. Gorby, S.B. Reed, D.E. Culley, C.L. Reardon, S. Barua, M.F. Romine, Applied and Environmental Microbiology (2007). AEM. 01087–01007v01081.
[21] Y. Zhang, G. Mo, X. Li, W. Zhang, J. Zhang, J. Ye, X. Huang, C. Yu, Journal of Power Sources (2011).

[22] W. Lee, C.H. Ahn, S. Hong, S. Kim, S. Lee, Y. Baek, J. Yoon, Journal of Membrane Science 351 (2010) 112–122.
[23] L. Zhang, X. Zhu, J. Li, Q. Liao, D. Ye, Journal of Power Sources (2011).
[24] L. Zhuang, C. Feng, S. Zhou, Y. Li, Y. Wang, Process Biochemistry 45 (2010) 929–934.
[25] M.A. Hickner, Transport and Structure in Fuel Cell Proton Exchange Membranes, Virginia Polytechnic Institute and State University, 2003.
[26] M.A. Hickner, H. Ghassemi, Y.S. Kim, B.R. Einsla, J.E. McGrath, Chemical Reviews 104 (2004) 4587–4612.
[27] Q. Li, M. Elimelech, Environmental Science & Technology 38 (2004) 4683–4693.
[28] J.C. Bendert, D.D. Papadias, D.J. Myers, Journal of the Electrochemical Society 157 (2010) B1486.
[29] F. Zhao, R.C.T. Slade, J.R. Varcoe, Chemical Society Reviews 38 (2009) 1926–1939.
[30] E. Marsili, D.B. Baron, I.D. Shikhare, D. Coursolle, J.A. Gralnick, D.R. Bond, Proceedings of the National Academy of Sciences 105 (2008) 3968.
[31] H.J. Kim, H.S. Park, M.S. Hyun, I.S. Chang, M. Kim, B.H. Kim, Enzyme and Microbial Technology 30 (2002) 145–152.
[32] D.K. Gosser, Cyclic Voltammetry: Simulation and Analysis of Reaction Mechanisms, Wiley-VCH, 1993.
[33] B.H. Kim, T. Ikeda, H.S. Park, H.J. Kim, M.S. Hyun, K. Kano, K. Takagi, H. Tatsumi, Biotechnology Techniques 13 (1999) 475–478.
[34] H. Von Canstein, J. Ogawa, S. Shimizu, J.R. Lloyd, Applied and Environmental Microbiology 74 (2008) 615–623.
[35] N. Uría, X. Muñoz Berbel, O. Sánchez, F.X. Muñoz, J. Mas, Environmental Science & Technology (2011).
[36] S. Pandit, A. Sengupta, S. Kale, D. Das, Bioresource Technology (2010).
[37] O. Bretschger, A. Cheung, F. Mansfeld, K.H. Nealson, Electroanalysis 22 (2010) 883–894.
[38] L. Huang, I. Angelidaki, Biotechnology and Bioengineering 100 (2008) 413–422.
[39] C. Feng, L. Ma, F. Li, H. Mai, X. Lang, S. Fan, Biosensors and Bioelectronics 25 (2010) 1516–1520.
[40] V.J. Watson, B.E. Logan, Biotechnology and Bioengineering 105 (2010) 489–498.
[41] Y.P. Chen, Y. Zhao, K.Q. Qiu, J. Chu, R. Lu, M. Sun, X.W. Liu, G.P. Sheng, H.Q. Yu, J. Chen, Biosensors and Bioelectronics (2010).
[42] A. Kouzuma, X.Y. Meng, N. Kimura, K. Hashimoto, K. Watanabe, Applied and Environmental Microbiology 76 (2010) 4151.
[43] S.B. Velasquez-Orta, I.M. Head, T.P. Curtis, K. Scott, J.R. Lloyd, H. von Canstein, Applied Microbiology and Biotechnology 85 (2010) 1373–1381.